# Propagation of a plane strain hydraulic fracture with a fluid lag in permeable rock

B. Chen [a, b], Andrew R Barron [a, c, d] and D.R.J. Owen [b], Chen-Feng Li [a, b, †]

[a] Energy Safety Research Institute, College of Engineering, Swansea University Bay Campus, Swansea SA1 8EN, U.K.

[b] Zienkiewicz Centre for Computational Engineering, College of Engineering, Swansea University Bay Campus, Swansea SA1 8EN, U.K.

[c] Department of Chemistry, Rice University, Houston, TX 77005, USA

[d] Department of Materials Science and Nanoengineering, Rice University, Houston, TX 77005, USA

**Abstract:** Based on the KGD scheme, this paper investigates, with both analytical and numerical approaches, the propagation of a hydraulic fracture with a fluid lag in permeable rock. On the analytical aspect, the general form of normalized governing equations is firstly formulated to take into account both fluid lag and leak-off during the process of hydraulic fracturing. Then a new self-similar solution corresponding to the limiting case of zero dimensionless confining stress ($\mathcal{T} = 0$) and infinite dimensionless leak-off coefficient ($\mathcal{L} = \infty$) is obtained. A dimensionless parameter $\mathcal{R}$ is proposed to indicate the propagation regimes of hydraulic fracture in more general cases, where $\mathcal{R}$ is defined as the ratio of the two time scales related to the dimensionless confining stress $\mathcal{T}$ and the dimensionless leak-off coefficient $\mathcal{L}$. In addition, a robust finite element based KGD model has been developed to simulate the transient process from $\mathcal{L} = 0$ to $\mathcal{L} = \infty$ under $\mathcal{T} = 0$, and the numerical solutions converge and agree well with the self-similar solution at $\mathcal{T} = 0$ and $\mathcal{L} = \infty$. More general processes from $\mathcal{T} = 0$ and $\mathcal{L} = 0$ to $\mathcal{T} = \infty$ and $\mathcal{L} = \infty$ for three different values of $\mathcal{R}$ are also simulated, which proves the effectiveness of the proposed dimensionless parameter $\mathcal{R}$ for indicating fracture regimes.

**Keywords:** Hydraulic fracture, self-similar solution, fluid lag, leak-off, parametric space

## 1. Introduction

Owing to the increasing adoption in the oil & gas industries, hydraulic fracturing has been extensively researched for nearly half a century, using analytical, experimental, and numerical approaches. An influential set of work is the systematic semi-analytical studies based on the KGD model [1-3], among others. These studies have led to the classification of different kinds of propagation regimes, as well as providing benchmarks for more advanced numerical studies. The KGD model was firstly developed by Khristianovic and Zheltov [4] and Geertsma and De Klerk [5], and then was improved by Detournay and his co-workers since 1999 [6]. The problem of hydraulic fracturing is significantly simplified with the following assumptions: 1) plane strain assumption and 2) fracture propagation along a straight line. With respect to governing equations, the elastic equation is used to model the rock deformation while Poiseuille's law and the continuity equation are adopted to simulate the fluid flow. The fluid can be Newtonian or non-Newtonian. Fracture propagation is controlled by the linear elastic fracture mechanics theory. Leak-off can

† Corresponding author

E-mail: c.f.li@swansea.ac.uk

be simulated using Carter's leak-off model or just ignored. As for boundary conditions, a constant injection flow rate is normally assumed. Despite the strict assumptions, the important characteristics including nonlocal character of elastic response and coupling between fluid flow and rock deformation are captured by the KGD model.

Spence and Sharp [7] conducted a pioneering work in this direction, and they derived the late-time solution without leak-off for lens-shaped and plane strain hydraulic fracturing under power law time-dependent or exponential time-dependent injection flow rate. They proposed the idea of scaling to derive the self-similar solutions for hydraulic fracture propagating in limiting propagation regimes. By using scaling, the key unknowns including fluid pressure, fracture width and length are all transferred to corresponding time-independent normalized parameters. In the meantime, the governing equations are also transformed into normalized governing equations. Then the analytical solution consisting of a particular solution and a general solution (a series of Chebyshev polynomials) can be solved using the method of continuation. This novel analytical solution strategy became popular and has been adopted in many subsequent studies. Other polynomial basis functions such as orthogonal Jacobi polynomials and ultraspherical polynomial (or Gegenbauer polynomial) have also been adopted [6, 8, 9]. Another way to solve the normalized fracture width and fluid pressure is to assume a piecewise linear profile for fluid pressure and then solve the related coefficients through numerical iteration [10, 11].

Based on the solution strategy described in [7], the propagation of deep-buried or shallow plane strain and penny-shaped hydraulic fracture as well as specific tip behaviors have been extensively studied [12, 13]. The scope of this paper is restricted in the deep-buried plane strain hydraulic fracture. According to the analytical analysis, the propagation regimes of a hydraulic fracture are mainly determined by three dimensionless parameters, namely the dimensionless toughness $\mathcal{K}$, the dimensionless confining stress $\mathcal{T}$ and the dimensionless leak-off coefficient $\mathcal{L}$ [1, 2, 10]. These three dimensionless parameters ranging from 0 to $\infty$ are functions of rock and fluid properties, in-situ stress conditions and treatment parameters. A wedge-shaped parametric space, shown in Figure 1(a), has been constructed considering the merging of early time ($\mathcal{T} = 1$) and late time ($\mathcal{T} \gg 1$) solutions for large dimensionless toughness [14]. Different combination of the values or evolutions of the three dimensionless parameters correspond to different propagation regimes. For example, $\mathcal{K} = \infty$, $\mathcal{T} = 0$ and $\mathcal{L} = 0$ corresponds to toughness-storage-dominated propagation of hydraulic fracture (vertex K). To summarize, the following cases have been investigated semi-analytically: 1) MK edge ($0 < \mathcal{K} < \infty$, $\mathcal{T} = \infty$ and $\mathcal{L} = 0$) [7]; 2) Vertex M ($\mathcal{K} = 0$, $\mathcal{T} = \infty$ and $\mathcal{L} = 0$) [6, 8]; 3) Vertex M ($\mathcal{K} = 1$, $\mathcal{T} = \infty$ and $\mathcal{L} = 0$) [9]; 4) K$\widetilde{\text{K}}$ edge ($\mathcal{K} = \infty$ and $0 \le \mathcal{L} < \infty$) [15, 16]; 5) Vertex O and K, edge OK ($0 \le \mathcal{K} < \infty, \mathcal{T} = 0$ and $\mathcal{L} = 0$) [10]; 6) Vertex K ($\mathcal{K} = 1$, $\mathcal{T} = 0$ and $\mathcal{L} = 0$) [3, 17]; 7) Plane OMK ($0 < \mathcal{K} < \infty, 0 < \mathcal{T} < \infty$ and $\mathcal{L} = 0$) [1]; 8) Vertex M, $\widetilde{\text{M}}$ and edge M$\widetilde{\text{M}}$ ($\mathcal{K} = 0, \mathcal{T} = \infty$ and $0 \le \mathcal{L} < \infty$) [2]; and 9) Plane MK$\widetilde{\text{M}}\widetilde{\text{K}}$ ($0 < \mathcal{K} < \infty, \mathcal{T} = \infty$ and $0 \le \mathcal{L} < \infty$) [11]. A comprehensive review of these solutions are presented in [13]. These existing semi-analytical solutions have served as benchmarks for extensive numerical algorithms [18-22]. More recently, Dontsov [23] derived the approximate solutions for all the vertices and edges on MK$\widetilde{\text{M}}\widetilde{\text{K}}$ plane and verified them with numerical solutions. Self-similar solutions with respect to porous media have also attracted increasing attention recently [24, 25].

Apart from the analytical investigations, the hydraulic fractures propagating in specific propagation regimes have also been simulated numerically. Desroches and Thiercelin [26] developed a hydraulic fracturing model named Loramec in KGD scheme. By using an integro-variational approach for the elasticity equation, both the fracture width and fluid pressure were expressed and solved on a 1D mesh. Fluid lag and leak-off have been simulated separately and the corresponding results have been used to verify the semi-analytical

solutions in literatures [6, 27]. Without considering leak-off, Hunsweck, Shen [28] developed an finite element based hydraulic fracturing model following the KGD scheme. The numerical results match well with the self-similar early-time and late-time solutions.

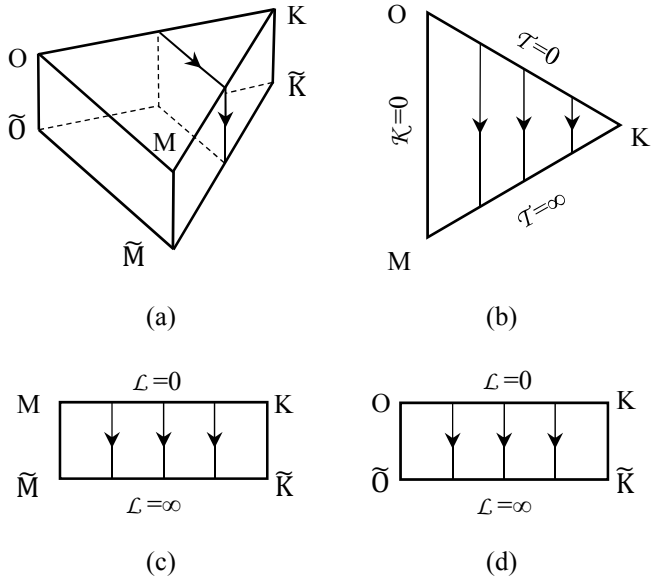


Figure 1. Parametric space of plane strain hydraulic fracturing and limiting propagation regimes

However, the previous analytical and numerical solutions all stay on OMK and MK$\widetilde{M}\widetilde{K}$ plane (shown in Figure 1(b) and Figure 1(c)). In this study, the self-similar solutions on $\widetilde{O}\widetilde{K}$ edge ($0<\mathcal{K}<\infty, \mathcal{T}=0$ and $\mathcal{L}=\infty$) are obtained with a semi-analytical approach, while the transient solution from OK edge to $\widetilde{O}\widetilde{K}$ edge (OK$\widetilde{O}\widetilde{K}$ Plane: $0<\mathcal{K}<\infty$, $\mathcal{T}=0$ and $0<\mathcal{T}<\infty$), shown in Figure 1(d), and the transient solution from OK edge to $\widetilde{M}\widetilde{K}$ edge are solved numerically. The current study differs from the previous studies in the sense that the fluid lag and leak-off need to be modelled simultaneously, which requires complete governing equations with both fluid lag and leak-off considered in the theoretical analysis and a robust numerical model to deal with related simulation issues due to significant decrease of fluid front velocity caused by leak-off. A new dimensionless parameter is proposed to indicate the propagation regimes of hydraulic fracture in more general cases. The rest of the paper is organized as follows. In Section 2, the problem formulation and governing equations are presented. In Section 3, the general form of the normalized equations suitable for the analysis of both fluid lag and leak-off is derived firstly. Then the relation between the dimensionless parameters and the possible propagation regimes of hydraulic fracturing are discussed. The asymptotic solutions for hydraulic fracturing under zero dimensionless confining stress and infinite dimensionless leak-off coefficient are solved. A finite element based KGD model is developed in Section 4. The semi-analytical and numerical results for the asymptotic and transient solutions are discussed and compared in Section 5.

## 2. Mathematical models

We base our study on a KGD model as shown in Figure 2, where a plane strain assumption is applied along the plane orthogonal to the vertical wellbore. The rock formation is assumed to be linear elastic, plane-strain and permeable. To simulate the fracturing fluid, the incompressible Newtonian fluid model is adopted with the laminar-flow assumption. The stress boundary conditions are set according to the confining stresses, while the influence from gravity is ignored as it is orthogonal to the simulation plane. A constant injection flow rate is imposed on the injection point at the center of the model. A strict assumption in the KGD model is that the hydraulic fracture propagates along a straight line. For the sake of completeness, the governing

equations for rock deformation, fluid flow and fracture propagation are briefly summarized below.

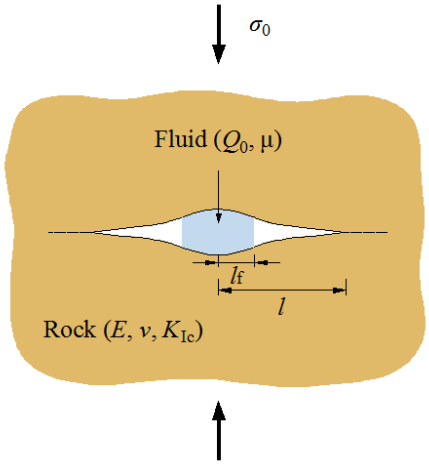


Figure 2. Sketch of the KGD model

Rock deformation is computed according to an elastic singular integral equation relating the net pressure $p = p_f - \sigma_0$ to fracture width and fluid pressure inside fluid lag is assumed to be zero.

$$w = \frac{1}{E'}\int_0^{l_f} G\left(\frac{x}{l},\frac{s}{l}\right) p\,ds - \frac{\sigma_0}{E'}\int_{l_f}^{l} G\left(\frac{x}{l},\frac{s}{l}\right) ds \tag{1}$$

where $E' = E/(1-v^2)$ is the plane strain modulus, $E$ and $v$ are the Young's modulus and Poisson's ratio of the rock respectively, $l$ is half length of the fracture, $l_f$ is half length of fluid channel and the integral kernel $G$ is expressed as

$$G(\xi,\eta) = \frac{4}{\pi}\ln\left|\frac{\sqrt{1-\xi^2}+\sqrt{1-\eta^2}}{\sqrt{1-\xi^2}-\sqrt{1-\eta^2}}\right| \tag{2}$$

As the width of a hydraulic fracture is much smaller than the other two dimensions, a lubrication theory, known as the Poiseuille's law (or the cubic law) is commonly adopted to describe the momentum conservation of fracturing fluid:

$$q = -\frac{w^3}{\mu'}\frac{\partial p_f}{\partial s} \tag{3}$$

where $q$ is the flow rate, $w$ the fracture width, $\mu'$=12$\mu$, $\mu$ the viscosity of the fracturing fluid, $p_f$ the fluid pressure, and $s$ is the local coordinate aligned with the tangential direction to the fracture path. Considering the leak-off, the mass conservation for fluid flow is expressed as:

$$\frac{\partial w}{\partial t} + \frac{\partial q}{\partial s} + g = 0 \tag{4}$$

where $\partial t$ denotes time derivative. Leak-off flow rate g is determined according to Carter's leak-off model:

$$g = \frac{C'}{\sqrt{t - t_0(s)}} \tag{5}$$

where $C' = 2C_L$, $C_L$ is the leak-off coefficient, $t_0$ is the time at which the fluid front arrived to a given point of coordinate $s$.

Substituting Eqn. (3) into Eqn. (4) yields

$$\frac{\partial w}{\partial t} - \frac{1}{12\mu}\frac{\partial}{\partial s}\left( w^3 \frac{\partial p_f}{\partial s} \right) + g = 0 \tag{6}$$

The corresponding boundary condition for this equation is a constant injection flow rate $Q_0$ at s=0. The integral form of the local continuity equation is expressed as

$$\frac{\partial}{\partial t}\int_s^{l_f} w ds + \int_s^{l_f} g ds = -\frac{w^3}{\mu'}\frac{\partial p_f}{\partial s} \tag{7}$$

The global continuity equation can be obtained by integrating equation (6) along the fracture length and time:

$$\frac{1}{2}Q_0 t = \int_0^{l_f} w ds + 2C'\int_0^{l_f} \sqrt{t - t_0(s)}\, ds \tag{8}$$

It is assumed that the hydraulic fracture propagates in mobile equilibrium which means the mode I stress intensity factor is always equal to the rock toughness $K_{Ic}$. The stress intensity factor $K_I$ is computed by

$$K_I = 2\sqrt{\frac{l}{\pi}}\left( \int_0^{l_f} \frac{p}{\sqrt{l^2 - x^2}} dx + \int_{l_f}^{l} \frac{-\sigma_0}{\sqrt{l^2 - x^2}} dx \right) \tag{9}$$

## 3. Asymptotic solutions

### 3.1 Normalized governing equations

Since the pioneering work [7], scaling has been adopted as an indispensable step in deducing analytical solutions for hydraulic fracturing to transfer the governing equations into dimensionless forms without time emerges. A common form of scaling can be expressed as [3]:

$$\begin{aligned} l(t) &= L\gamma \\ p(x,t) &= \varepsilon E' \Pi \\ w(x,t) &= \varepsilon L \Omega \end{aligned} \tag{10}$$

where $L$ is a length scale, $\varepsilon$ is a small factor, $\xi$, $\gamma$, $\Pi$ and $\Omega$ are normalized coordinate along fracture, normalized fracture length, normalized net-pressure and normalized fracture width.

Introducing the scaling equations (10) into the governing equations (5-9) results in a set of normalized

governing equations.

- Normalized elastic equation

$$\frac{\Omega}{\gamma}=\int_0^{\xi_f} G\left(\xi,\xi'\right)\Pi\left(\xi',t\right)d\xi'-\mathcal{T}\int_{\xi_f}^{1} G\left(\xi,\xi'\right)d\xi',\quad \xi\in(0,1) \tag{11}$$

- Normalized Poiseuille's law

$$\mathcal{G}_v\left[\left(\frac{t\dot{\gamma}}{\gamma}+\frac{t\dot{\varepsilon}}{\varepsilon}+2\frac{t\dot{L}}{L}\right)\int_{\xi}^{\xi_f}\Omega d\xi+t\Omega_f\dot{\xi}_f+\Omega\xi\left(\frac{t\dot{\gamma}}{\gamma}+\frac{t\dot{L}}{L}\right)+\int_{\xi}^{\xi_f}t\dot{\Omega}d\xi\right]+\mathcal{G}_c\int_{\xi}^{\xi_f}\Gamma d\xi=-\frac{1}{\mathcal{G}_m}\frac{\Omega^3}{\gamma^2}\frac{\partial\Pi}{\partial\xi},\quad \xi\in(0,\xi_f) \tag{12}$$

$\Gamma=1/\sqrt{1-\theta(\xi)}$, $\theta(\xi)=t_0/t$ is the normalized arrival time of fluid front remaining to be determined.

The corresponding boundary condition in the lag is

$$\Pi=-\mathcal{T},\quad \xi\in[\xi_f,1] \tag{13}$$

- Global continuity equation

$$\frac{1}{2\gamma}=\mathcal{G}_v\int_0^{\xi_f}\Omega d\xi+2\mathcal{G}_c\int_0^{\xi_f}\sqrt{1-\theta(\xi)}d\xi \tag{14}$$

- Fracture propagation criterion

$$\mathcal{G}_k=\frac{2^{7/2}}{\pi}\gamma^{1/2}\left(\int_0^{\xi_f}\frac{\Pi d\xi}{\sqrt{1-\xi^2}}-\mathcal{T}\arccos\xi_f\right) \tag{15}$$

where $$\mathcal{G}_v=\frac{\varepsilon L^2}{Q_0 t},\ \mathcal{G}_c=\frac{C'L}{Q_0 t^{1/2}},\ \mathcal{G}_m=\frac{Q_0\mu'}{\varepsilon^4 L^2 E'},\ \mathcal{G}_k=\frac{K'}{\varepsilon E' L^{1/2}}\ \text{and}\ \mathcal{T}=\frac{\sigma_0}{\varepsilon E'} \tag{16}$$

$\xi_f=l_f/l$ is the fluid fraction, the small factor $\varepsilon$ and the length scale $L$ are still to be determined according to the specific propagation regimes to be solved and $K'=4\sqrt{2/\pi}K_{\mathrm{Ic}}$

### 3.2 Propagation regimes

Represented by solutions $\{\Omega,\Pi,\gamma,\xi_f\}$ for equation (11)-(15), the behavior of hydraulic fracturing differs under different conditions described by the five dimensionless parameters. The dimensionless parameters can be divided into three groups: 1) $\mathcal{G}_m$ and $\mathcal{G}_k$; 2) $\mathcal{T}$ and 3) $\mathcal{G}_v$ and $\mathcal{G}_c$. The factors $\mathcal{G}_v$ and $\mathcal{G}_c$ reflect whether the fluid storage or leak-off dominates the hydraulic fracturing process while the factors $\mathcal{G}_m$ and $\mathcal{G}_k$

reflect the energy dissipated on driving viscous fluid and fracturing rock. In order to analyze how the input parameters influence hydraulic fracturing behaviors through dimensionless parameters, explicit expressions of dimensionless parameters need to be determined. Without loss of generality, we restrict $\mathcal{G}_m=1$ and $\mathcal{G}_v=1$. After solving the scaling parameters $L$ and $\varepsilon$, the other three dimensionless parameters can be expressed as

$$\mathcal{K}=\mathcal{G}_k=K'\left(\frac{1}{Q_0E'^3\mu'}\right)^{1/4},\quad \mathcal{T}=\sigma_0\left(\frac{t}{E'^2\mu'}\right)^{1/3},\quad \mathcal{L}=\mathcal{G}_c=C'\left(\frac{E't}{\mu'Q_0^3}\right)^{1/6} \tag{17}$$

The three dimensionless parameters ranging from 0 to $\infty$ constitute a wedge-shaped parametric space, shown in Figure 1(a). The dimensionless toughness $\mathcal{K}$ is independent of time while both the dimensionless confining stress $\mathcal{T}$ and dimensionless leak-off coefficient $\mathcal{L}$ are dynamic parameters evolving with time. In addition, it is assumed that $\mathcal{K}$ varies from 0 at OM$\tilde{\text{O}}\tilde{\text{M}}$ to $\infty$ at K$\tilde{\text{K}}$, $\mathcal{T}$ increases from 0 at OK$\tilde{\text{O}}\tilde{\text{K}}$ to $\infty$ at MK$\tilde{\text{M}}\tilde{\text{K}}$, and $\mathcal{L}$ increases from 0 at OMK to $\infty$ at $\tilde{\text{O}}\tilde{\text{M}}\tilde{\text{K}}$. In this case, each hydraulic fracturing process corresponds to a path on a plane parallel to OM$\tilde{\text{O}}\tilde{\text{M}}$, as shown in Figure 1 (a). All the paths evolve from a specific point at OK ($\mathcal{T}=0$ and $\mathcal{L}=0$) to $\tilde{\text{M}}\tilde{\text{K}}$ ($\mathcal{T}=\infty$ and $\mathcal{L}=\infty$) but also vary with each other depending on the relative magnitude of the two time scale related to $\mathcal{T}$ and $\mathcal{L}$ respectively:

$$\mathcal{R}=\frac{t_l}{t_\sigma}=\frac{\mu'Q_0^3}{E'C'^6}\Big/\frac{E'^2\mu'}{\sigma_0^3}=\left(\frac{\sigma_0Q_0}{E'C'^2}\right)^3 \tag{18}$$

In the case $\mathcal{R}$ ? 1, hydraulic fracturing evolves from OK edge to MK edge firstly and then to $\tilde{\text{M}}\tilde{\text{K}}$ edge. Conversely, it evolves from OK edge to $\tilde{\text{O}}\tilde{\text{K}}$ edge and then to $\tilde{\text{M}}\tilde{\text{K}}$ edge in case of $\mathcal{R}=1$. In more general cases $\mathcal{R}$ is slightly over 1 (or below 1), hydraulic fracturing gets closer to MK edge (or $\tilde{\text{O}}\tilde{\text{K}}$ edge) firstly and then evolves to $\tilde{\text{M}}\tilde{\text{K}}$ edge. Therefore, each pair of $\mathcal{K}$ and $\mathcal{R}$ corresponds to a unique path of hydraulic fracturing, and the state of the hydraulic fracturing (i.e. a point on the path) can be further determined once either $\mathcal{T}$ or $\mathcal{L}$ is known.

### 3.3 Scaling schemes

As shown in Figure 1(a), there are four limiting propagation regimes: OK edge, $\tilde{\text{O}}\tilde{\text{K}}$ edge, MK edge and $\tilde{\text{M}}\tilde{\text{K}}$ edge. The asymptotic solutions at OK edge, MK edge and $\tilde{\text{M}}\tilde{\text{K}}$ edge have been reported in literatures [7, 10, 11], while the remaining asymptotic solution at $\tilde{\text{O}}\tilde{\text{K}}$ edge is obtained in this study. At $\tilde{\text{O}}\tilde{\text{K}}$ edge, the propagation of hydraulic fracture is dominated by leak-off, hence $\mathcal{G}_c=1$. For the sake of convenience, the viscosity scaling is chosen here, i.e. $\mathcal{G}_m=1$. Thus the scaling parameters can be expressed as

$$\varepsilon=\left(\frac{\mu'C'^2}{E'Q_0t}\right)^{1/4},\quad L=\left(\frac{Q_0^2t}{C'^2}\right)^{1/2} \tag{19}$$

Thus

$$\mathcal{G}_v=\left(\frac{\mu'Q_0^3}{E'C'^6t}\right)^{1/4},\quad \mathcal{K}=\mathcal{G}_k=K'\left(\frac{1}{Q_0E'^3\mu'}\right)^{1/4},\quad \mathcal{T}=\sigma_0\left(\frac{t}{E'^2\mu'}\right)^{1/3} \tag{20}$$

For $\widetilde{0}\widetilde{K}$ edge, $\frac{\mu' Q_0^{\ 3}}{E' C'^6} = t = \frac{E'^2 \mu'}{\sigma_0^3}$, therefore

$$\mathcal{G}_v = 0, \quad \mathcal{T} = 0 \tag{21}$$

### 3.4 Semi-analytical solutions

Substituting $\mathcal{G}_c = \mathcal{G}_m = 1$ and equations (19) and (21) into the normalized equations (11)-(15) and re-scaling the normalized $\Omega$ and $\Pi$ using $\bar{\Omega} = \Omega \gamma^{-3/4}$, $\bar{\Pi} = \Pi \gamma^{1/4}$ to eliminate the normalized fracture length $\gamma$ in equation (12) and (14) lead to:

- Normalized elastic equation

$$\bar{\Omega} = \int_0^{\xi_f} G(\xi, \xi') \bar{\Pi}(\xi', t) d\xi', \quad \xi \in (0,1) \tag{22}$$

- Normalized Poiseuille's law

$$\int_{\xi}^{\xi_f} \Gamma d\xi = \bar{\Omega}^3 \frac{\partial \bar{\Pi}}{\partial \xi}, \quad \xi \in (0, \xi_f) \tag{23}$$

where $\Gamma = 1/\sqrt{1-\theta(\xi)^2}$, considering $l: t^{1/2}$ and $x/\xi_f: t_0^{1/2}$, $\theta(\xi) = t_0/t = ((x/\xi_f)/l)^2 = (\xi/\xi_f)^2$

Corresponding boundary condition in the lag is

$$\bar{\Pi} = 0, \quad \xi \in [\xi_f, 1] \tag{24}$$

- Global continuity equation

$$\frac{1}{2\gamma} = 2\int_0^{\xi_f} \sqrt{1-\theta(\xi)} d\xi \tag{25}$$

- Fracture propagation criterion

$$\mathcal{K} = \frac{2^{7/2}}{\pi} \gamma^{1/2} \left( \int_0^{\xi_f} \frac{\Pi d\xi}{\sqrt{1-\xi^2}} - \mathcal{T} \arccos \xi_f \right) \tag{26}$$

The self-similar solutions $\{\Omega, \Pi, \gamma, \xi_f\}$ is the function of dimensionless toughness $\mathcal{K}$ and crack coordinate $\xi$. In order to avoid solving the governing equations in a priori unknown domain, the first three equations are solved firstly with a given value of $\xi_f$. More specifically, the normalized fracture length can be solved explicitly according to equation (25) and the normalized fracture width and fluid pressure are solved using a

numerical process detailed in [10]. Once the normalized fracture length, fracture width and fluid pressure are determined, the dimensionless toughness corresponding to these solutions can be computed. These results are discussed in Section 5.

# 4. Numerical model

## 4.1 Finite element scheme

The finite element method is adopted to solve the rock deformation. The weak form of the equilibrium equation is:

$$\int_{\Lambda} \delta\varepsilon_{ij} c_{ijrs} \varepsilon_{rs} d\Lambda - \int_{\Gamma_e} \delta u_i t_i d\Gamma_e - \int_{\Gamma} \delta u_i p_i d\Gamma = 0 \tag{27}$$

where $\Lambda$ is the domain of surrounding medium, $\Gamma_e$ is the external boundary, $p$ and $\Gamma$ are the fluid pressure and the 1D fracture path respectively. $\delta\varepsilon_{ij}$ is the strain corresponding to virtual displacement $\delta u_i$.

The fluid equation (6) can be solved with any fluid solver, such as the finite difference, finite element or finite volume schemes. In our implementation, to accurately track the fluid front in relation to the fracture tip and to simplify mesh operations, we take a finite element approach for the fluid solution as well. Specifically, the weak form of Eqn. (6) is

$$\int_{\Gamma} \delta p \frac{\partial w}{\partial t} d\Gamma + \int_{\Gamma} (\delta p)_{,s} \frac{w^3}{12\mu} p_{,s} d\Gamma - \delta p(0) q(0) + \delta p(s_f) q(s_f) + \int_{\Gamma} g d\Gamma = 0 \tag{28}$$

where $p(0)$ and $q(0)$ are the fluid pressure and the flow rate at the injection point (i.e. fracture center), and $p(s_f)$ and $q(s_f)$ are the fluid pressure and the flow rate at the fluid front. A constant injection flow rate $q(0)$ is assumed at the center of the initial fracture. The pressure at the fluid lag is set to zero, i.e. $p(s_f) = 0$.

## 4.2 Spatial and temporal discretization

Following the symmetry of the KGD model, only a quarter of the whole domain is considered, as shown in Figure 3. At the beginning of the simulation, the finite element simulation domain is set as $50L_0$ by $50L_0$ (i.e. $a$=$50L_0$) to approximate the infinite rock formation ($L_0$ is the initial half-length of fracture). A uniform and fine mesh is applied on the boundary from (0, 0) to ($2.5L_0$, 0), as shown in Figure 4. Once the fracture length doubles, the computation domain is also doubled to keep the fracture stay in the range [a/50, a/25], which makes the approximation of infinite medium always satisfied. The solution information on the old mesh needs to be transferred to the new mesh once the mesh changes.

The fluid front and the fracture tip are both restricted to the element node during simulation. In each time step, the fluid front is updated firstly and then the crack tip is updated step by step along the bottom boundary until the fracture criterion is not satisfied. In this case, remeshing is avoided by updating the boundary condition according to the position of fluid front and crack tip. As for the time step $\Delta t$, it is normally determined according to the fluid front velocity explicitly, i.e. $\Delta t = d / v_f^{(n)}$ where $d$ is the advancement limit specified by the user and $v_f^{(n)}$ is the fluid front velocity at last time step. However, it is found from our numerical test that the explicit time step leads to unstable fluid front velocity in the case of

very small fluid front advance velocity due to significant leak-off. Here the time step is determined implicitly using $\Delta t = 2d/(v_f^{(n)} + v_f^{(n+1)})$ where $v_f^{(n+1)}$ is the fluid front velocity at next time step, $d$ could be one or several times of the minimum mesh size (3 by default in our simulations). Instead of using an explicit time step, we update the time step when solving the elastic equations and fluid flow equation once the pre-set convergence criteria is met, and the algorithm flow is described in Section 4.4.

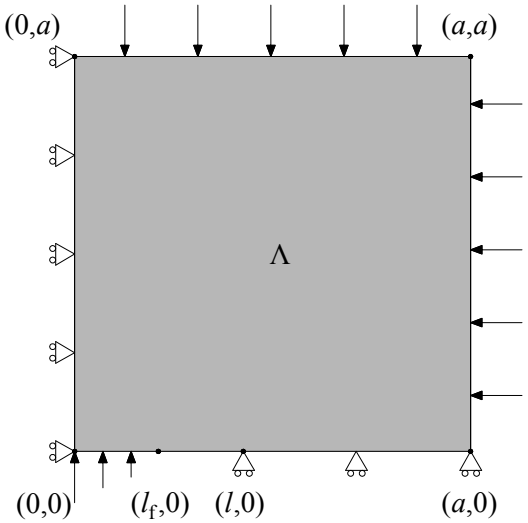


Figure 3. Computational model for quarter of the KGD-scheme. The injection point locates in the origin. ($l$, 0) and ($l_f$, 0) are the location of crack tip and fluid front respectively. $a$ is 50 times of the initial fracture length at the beginning of the simulation and doubles when a <25$l$.

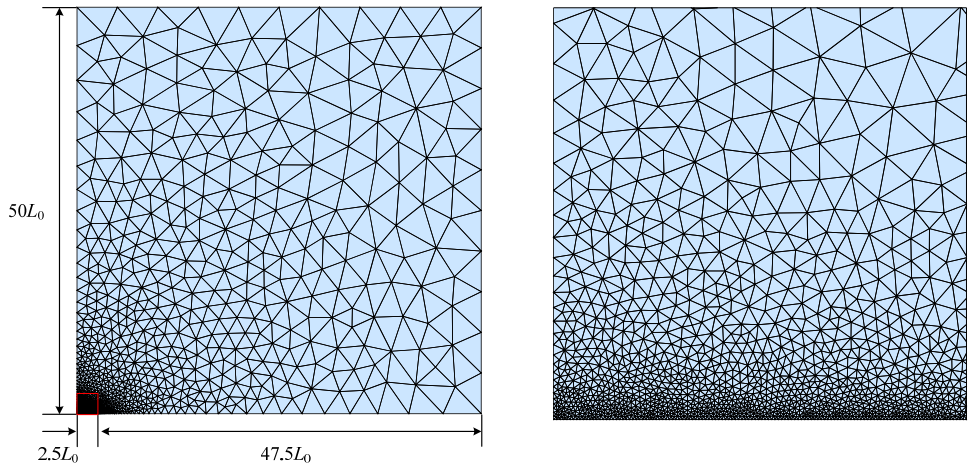


Figure 4. Finite element mesh used for numerical simulation. Left: the entire simulation domain. Right: the mesh between (0, 0) and (2.5$L_0$, 0).

### 4.3 Strongly-coupled finite element solution

As shown in equation (27) and (28), the displacement field **u** is coupled with the fluid pressure **p**. In the following part, a strongly-coupled solution process for nodal displacement $\mathbf{u}_{m+1}$ and the nodal pressure $\mathbf{p}_{m+1}$ at time $t_{m+1}$ based on the nodal displacement $\mathbf{u}_m$ and the nodal pressure $\mathbf{p}_m$ at time $t_m$ is explained.

At time $t_{m+1}$, Eqn. (27) can be discretized as:

$$\mathbf{K}\mathbf{u}_{m+1} = \mathbf{F}(\mathbf{p}_{m+1}) + \mathbf{F}_{external} \tag{29}$$

where $\mathbf{K}$ is the stiffness matrix, $\mathbf{F}_{external}$ is nodal force at the domain boundary due to the confining stress of rock formations, and $\mathbf{F}(\mathbf{p}_{m+1})$ is the nodal force on the fracture due to the fluid pressure, expressed as

$$\mathbf{F}(\mathbf{p}_{m+1}) = \mathbf{T}\mathbf{p}_{m+1} \tag{30}$$

where $\mathbf{T}$ is a coefficient matrix computed from the 1D fluid mesh. For a linear uniform mesh, $\mathbf{T}$ has the following form

$$\mathbf{T} = \sum_e \mathrm{T}_{ij}^{(e)}\ ,\ \mathrm{T}_{ij}^{(e)} = \frac{l^e}{6}\begin{bmatrix} 2 & 1 \\ 1 & 2 \end{bmatrix} \tag{31}$$

where $l^e$ is the element length of the fluid mesh.

Discretizing Eqn. (28) with 1D linear finite elements yields:

$$\mathbf{L}\cdot(\mathbf{w}_{m+1} - \mathbf{w}_m)/(t_{m+1} - t_m) + \mathbf{h}(\mathbf{w}_{m+1}, \mathbf{p}_{m+1}) + \mathbf{g}(t_{m+1}, \mathbf{t}_0) = \mathbf{q}_{m+1} \tag{32}$$

where $\mathbf{w}_{m+1}$ and $\mathbf{w}_m$ are the nodal fracture widths at time $t_{m+1}$ and $t_m$ respectively, $\mathbf{L}$ is a coefficient matrix, $\mathbf{h}(\mathbf{w}_{m+1}, \mathbf{p}_{m+1})$ is a nonlinear vector function with respect to the nodal fracture width $\mathbf{w}_{m+1}$ and the nodal fluid pressure $\mathbf{p}_{m+1}$, $\mathbf{g}(t_{m+1}, \mathbf{t}_0)$ is a vector function with respect to the time $t_{m+1}$ and the nodal exposed time $\mathbf{t}_0$, and $\mathbf{q}_{m+1}$ is the nodal flow rate at time $t_{m+1}$. The fracture path is discretized into $N$ linear elements of lengths $\{l_1, l_2, \mathrm{L}\ l_N\}$ indexed from the crack center to the crack tip, and the first $N_f$ elements are occupied by the fracturing fluid. The matrix quantities in Eqn. (32) are defined as follows:

$$\mathbf{w} = \left[w_1, w_2, \mathrm{L}\ , w_i, \mathrm{L}\ , w_{N_f+1}\right]^T \tag{33a}$$

$$\mathbf{p} = \left[p_1, p_2, \mathrm{L}\ , p_i, \mathrm{L}\ , p_{N_f+1}\right]^T \tag{33b}$$

$$\mathbf{L} = \mathbf{T}(1 : N_f + 1, :) \tag{33c}$$

$$\mathbf{q}_{m+1} = \left[q(0), 0, \mathrm{L}\ , 0, q(N_f + 1)\right]^T \tag{33d}$$

$$\mathbf{h} = \begin{bmatrix} 0 \\ \hat{\mathbf{h}} \end{bmatrix} - \begin{bmatrix} \hat{\mathbf{h}} \\ 0 \end{bmatrix} \tag{33e}$$

$$\mathbf{g} = \begin{bmatrix} 0 \\ \hat{\mathbf{g}} \end{bmatrix} - \begin{bmatrix} \tilde{\mathbf{g}} \\ 0 \end{bmatrix} \tag{33f}$$

where the pressure at the fluid front is set to zero, i.e. $p_{N_f+1} = 0$. $\hat{\mathbf{h}} = \left[h_1, h_2, \cdots, h_i, \cdots, h_{N_f}\right]^T$ and

$h_i = \frac{1}{48\mu}\frac{p_{i+1}-p_i}{l_i}(w_i^2 + w_{i+1}^2)(w_i + w_{i+1})$ . $\hat{\mathbf{g}} = \left[\hat{g}_1, \hat{g}_2, \cdots, \hat{g}_i, \cdots, \hat{g}_{N_f}\right]^T$ and $\tilde{\mathbf{g}} = \left[\tilde{\mathrm{g}}_1, \tilde{\mathrm{g}}_2, \cdots, \tilde{\mathrm{g}}_i, \cdots, \tilde{\mathrm{g}}_{N_f}\right]^T$,

$$\hat{g}_i = C' l_i \frac{2}{3(\mathbf{t}_0(i) - \mathbf{t}_0(i+1))^2}\left[(3\mathbf{t}_0(i) - \mathbf{t}_0(i+1) - 2t)\sqrt{t - \mathbf{t}_0(i+1)} + 2(t - \mathbf{t}_0(i))^{3/2}\right] \tag{34a}$$

$$\tilde{\mathrm{g}}_i = C' l_i \frac{2}{3(\mathbf{t}_0(i) - \mathbf{t}_0(i+1))^2}\left[(3\mathbf{t}_0(i+1) - \mathbf{t}_0(i) - 2t)\sqrt{t - \mathbf{t}_0(i)} + 2(t - \mathbf{t}_0(i+1))^{3/2}\right] \tag{34b}$$

Therefore, following a finite element approach, the solid equation (27) and the fluid equation (28) are discretized into finite element equations (29) and (32) respectively, where the nodal fracture width $\mathbf{w}$ can be directly represented by the nodal displacement $\mathbf{u}$. The FE equations (29) and (32) are nonlinear and strongly coupled, and the Newton-Raphson scheme is adopted for their solution:

$$\begin{bmatrix}\mathbf{u}\\ \mathbf{p}\end{bmatrix}^{(n+1)} = \begin{bmatrix}\mathbf{u}\\ \mathbf{p}\end{bmatrix}^{(n)} - \mathbf{M}_{Jacobi} \backslash \mathbf{R} \tag{35}$$

where $n$ denotes the iteration step, $\mathbf{M}_{Jacobi}$ is the Jacobi matrix, and $\mathbf{R}$ is the residual vector. The Jacobi matrix and the residual vector are given below:

$$\mathbf{M}_{Jacobi} = \begin{bmatrix}\mathbf{K} & -\mathbf{J}\\ \left(\mathbf{L} + \frac{\partial \mathbf{h}}{\partial \mathbf{w}}\right)\frac{\partial \mathbf{w}}{\partial \mathbf{u}} & \frac{\partial \mathbf{h}}{\partial \mathbf{p}}\end{bmatrix} \tag{36a}$$

$$\mathbf{R} = \begin{bmatrix}\mathbf{K}\mathbf{u}^{(n)} - \mathbf{F}(\mathbf{p}^{(n)})\\ \mathbf{L}\cdot(\mathbf{w}^{(n)} - \mathbf{w}_m) + \mathbf{h}(\mathbf{w}^{(n)}, \mathbf{p}^{(n)}) - \mathbf{q}_{m+1}\end{bmatrix} \tag{36b}$$

where $\mathbf{J} = \mathbf{T}\left(:, 1{:}N_f\right)$.

### 4.4 Algorithm flow

For clarity, the overall algorithm flow of the proposed simulation strategy is summarized below:

Initial condition
**Repeat**
  Fluid front update
  **Repeat**
    Crack tip update
    Solving the coupled problem iteratively
      a) Elastic equation and fluid flow equations (poiseuille's law and continuity equation)
      b) Update the time step according to the new fluid front velocity
    Compute the stress intensity factor
  **Until** fracture criterion is not satisfied
  t ← t+Δt
**Until** end of simulation

Initial condition of the numerical simulation is set according to the self-similar solution at OK edge. After the advancement of fluid front in each time step, the fracture tip is updated until the computed stress intensity factor is lower than the rock toughness. The stress intensity factor is computed using interaction energy integral method [28, 29].

## 5. Results and discussion

The semi-analytical and the numerical solution strategies have been described in Section 3 and Section 4 respectively, and the corresponding solutions are presented in this section. In Section 5.1, a series of solutions for different values of dimensionless toughness $\mathcal{K}$ (i.e. a series of points on $\widetilde{\mathrm{OK}}$ edge) are obtained. The self-similar solution at $\mathcal{K} = 0.498$ is verified with the numerical results in Section 5.2, in which the transient process from OK edge to $\widetilde{\mathrm{OK}}$ edge is simulated numerically. In Section 5.3, the more general processes from OK edge to $\widetilde{\mathrm{MK}}$ edge for three different values of dimensionless parameter $\mathcal{R}$ are simulated, which proves the effectiveness of the proposed dimensionless parameter.

### 5.1 Asymptotic solution at $\widetilde{\mathrm{OK}}$ edge

The self-similar solutions $\{\Omega, \Pi, \gamma, \xi_{\mathrm{f}}\}$ corresponding to different dimensionless toughness at $\widetilde{\mathrm{OK}}$ edge have been solved from (22-26) with the methodology explained in Section 3.4 and are listed in Table 1. The normalized fracture length is solved explicitly through equation (25):

$$\gamma = 1/(\pi\xi_{\mathrm{f}}) \tag{37}$$

Profile of the normalized fracture width and fluid pressure under various value of fluid fraction are shown in Figure 5 and Figure 6.

Table 1 Dimensionless toughness $\mathcal{K}$ , fracture length $\gamma$ , fluid pressure at the inlet $\Pi(0)$ and fracture width at the inlet $\Omega(0)$ under various fluid fraction $\xi_{\mathrm{f}}$

| $\xi_{\mathrm{f}}$ | $\mathcal{K}$ | $\gamma$ | $\Pi(0)$ | $\Omega(0)$ |
|---|---|---|---|---|
| 0.001 | 0.0068 | 318.31 | 0.2440 | 4.6803 |
| 0.01 | 0.0275 | 31.831 | 0.3019 | 0.8019 |
| 0.03 | 0.0554 | 10.610 | 0.3425 | 0.7420 |
| 0.1 | 0.1250 | 3.1831 | 0.4060 | 0.7161 |
| 0.2 | 0.2077 | 1.5915 | 0.4582 | 0.7051 |
| 0.3 | 0.2862 | 1.0610 | 0.4977 | 0.7006 |
| 0.4 | 0.3660 | 0.7958 | 0.5318 | 0.6995 |
| 0.5 | 0.4507 | 0.6366 | 0.5631 | 0.7011 |
| 0.6 | 0.5444 | 0.5305 | 0.5931 | 0.7056 |
| 0.7 | 0.6536 | 0.4547 | 0.6232 | 0.7137 |
| 0.8 | 0.7908 | 0.3979 | 0.6547 | 0.7279 |
| 0.9 | 0.9928 | 0.3537 | 0.6914 | 0.7552 |
| 0.97 | 1.2741 | 0.3282 | 0.7296 | 0.8031 |
| 0.99 | 1.4759 | 0.3215 | 0.7524 | 0.8424 |
| 0.999 | 1.7881 | 0.3186 | 0.7875 | 0.9091 |

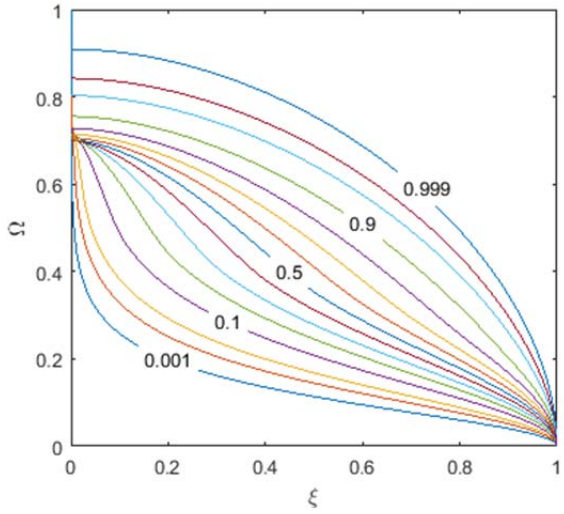


Figure 5. Self-similar solutions of normalized fracture width on $\widetilde{\mathrm{O}}\widetilde{\mathrm{K}}$ edge for various values of $\xi_f$ from 0.001 to 0.999 (corresponding values are shown in Table 1)

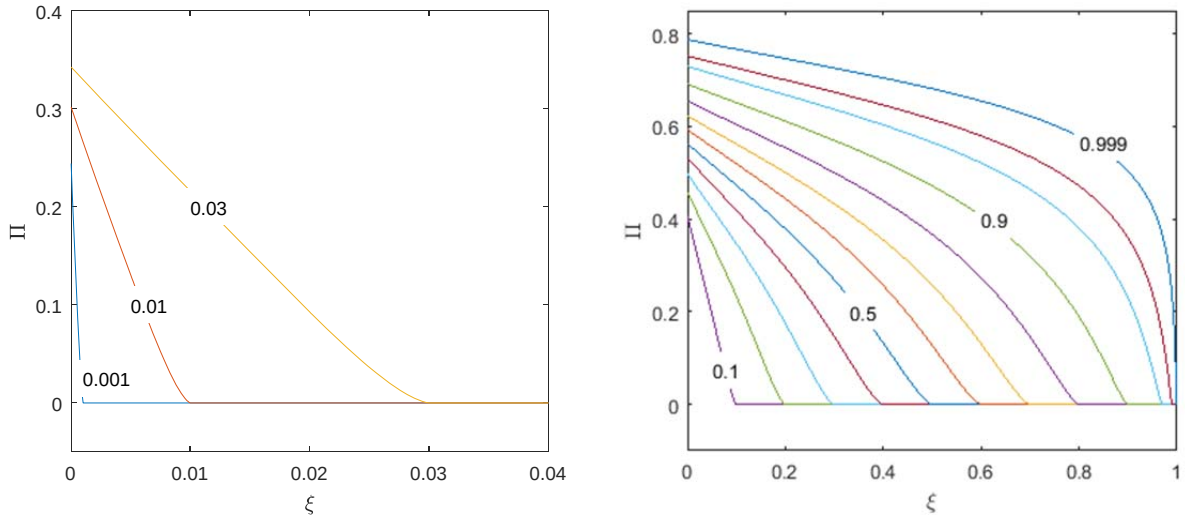


Figure 6. Self-similar solutions of normalized fluid pressure on $\widetilde{\mathrm{O}}\widetilde{\mathrm{K}}$ edge for various values of $\xi_f$ (corresponding values are shown in Table 1). Left: 0.001 to 0.03 and Right: 0.1 to 0.999.

### 5.2 Approximation of numerical solutions to self-similar solution at $\widetilde{\mathrm{O}}\widetilde{\mathrm{K}}$ edge

In this case $t_\sigma \gg t_l$, hydraulic fracturing evolves from OK edge to $\widetilde{\mathrm{O}}\widetilde{\mathrm{K}}$ edge firstly and then to $\widetilde{\mathrm{M}}\widetilde{\mathrm{K}}$ edge. The first stage of the process (shown in Figure 1 (d)) is simulated numerically using the finite element model detailed in Section 4. Different values of dimensionless toughness correspond to the different trajectories starting from OK edge and ending at $\widetilde{\mathrm{O}}\widetilde{\mathrm{K}}$ edge. Without loss of generality, we consider the case $\mathcal{K} = 0.498$. The initial state of the numerical simulation is set to be the asymptotic solution at OK edge. In order to keep the process in the Plane OK$\widetilde{\mathrm{O}}\widetilde{\mathrm{K}}$, the confining stress $\sigma_0$ is set to be zero. The related parameters used in the

simulation are listed in Table 2.

Table 2 Rock properties, fluid properties and loading conditions used in numerical simulation

| Rock properties | | Fluid properties | | Loading conditions | |
|---|---|---|---|---|---|
| Elastic modulus $E$ | 25GPa | Viscosity $\mu$ | 1cp | | |
| Poisson ratio $\nu$ | 0.3 | Flow rate $Q_0$ | 0.004m$^2$/s | Confining stress $\sigma_0$ | 0MPa |
| Toughness $K_{Ic}$ | 0.876MPa • m$^{1/2}$ | Leak-off coefficient $C_L$ | 0.0001m/s$^{1/2}$ | | |

The evolution of the fracture length is shown in Figure 7 and is compared with the limiting propagation regimes at OK edge and $\widetilde{\mathrm{O}}\widetilde{\mathrm{K}}$ edge. In the case $\mathcal{K}=0.498$, evolutions of the fracture half-length in the two different limiting propagation regimes could be expressed as

$$l = L\gamma = \begin{cases} 1.192\left(\dfrac{Q_0^3 E' t^4}{\mu'}\right)^{1/6} & \text{OK edge} \\ 0.579\left(\dfrac{Q_0^2 t}{C'^2}\right)^{1/2} & \tilde{\mathrm{O}}\tilde{\mathrm{K}} \text{ edge} \end{cases} \tag{38}$$

The dimensionless form of the results are

$$l/l_* = \begin{cases} 1.192(t/t_*)^{2/3} & \text{OK edge} \\ 0.579(t/t_*)^{1/2} & \tilde{\mathrm{O}}\tilde{\mathrm{K}} \text{ edge} \end{cases} \quad \text{where } t_* = \frac{\mu' Q_0^3}{E' C'^6},\ l_* = \left(\frac{\mu' Q_0^5}{E' C'^8}\right)^{1/2} \tag{39}$$

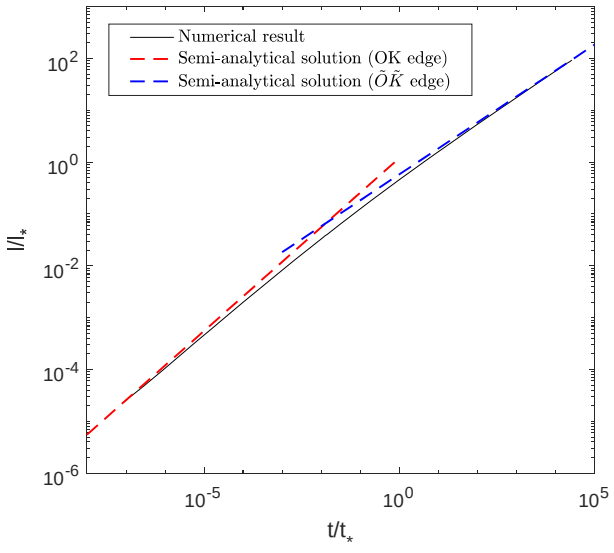


Figure 7. Evolution of the normalized fracture half-length with respect to dimensionless time under zero dimensionless confining stress

It is indicated from Figure 7 that fracture length evolves according to the asymptotic solution at OK edge at early-time stage and then approximates to the asymptotic solution at $\widetilde{\mathrm{O}}\widetilde{\mathrm{K}}$ edge with time elapsed. In order to verify the numerical results with the self-similar solutions at $\widetilde{\mathrm{O}}\widetilde{\mathrm{K}}$ edge, the fracture width and fluid pressure solved in numerical simulation are normalized according to equation (10) and (19) and are plotted in Figure

8. It is shown from Figure 8 that the normalized fracture width and fluid pressure approximate to the self-similar solution at $\tilde{O}\tilde{K}$ edge with the time elapsed, which verifies the accuracy of the solutions. Evolution of the fluid fraction from OK edge to $\tilde{O}\tilde{K}$ edge and the stress intensity factor computed at each time step are plotted in Figure 9. In both of the limiting state at OK edge and $\tilde{O}\tilde{K}$ edge, the fluid fraction is constant according to the theoretical analysis. As shown in Figure 9, the fluid fraction increase from 0.5 at OK edge to around 0.55 at $\tilde{O}\tilde{K}$ edge. A zig-zag curve is observed due to that the mobile equilibrium of fracture propagation, i.e. $K_I=K_{Ic}$, is not always exactly satisfied. But, as shown in Figure 9 (b), the error is kept below 2% during the simulation. The accuracy could be improved by using a finer mesh and increasing the step size of fluid front advancement at each time step.

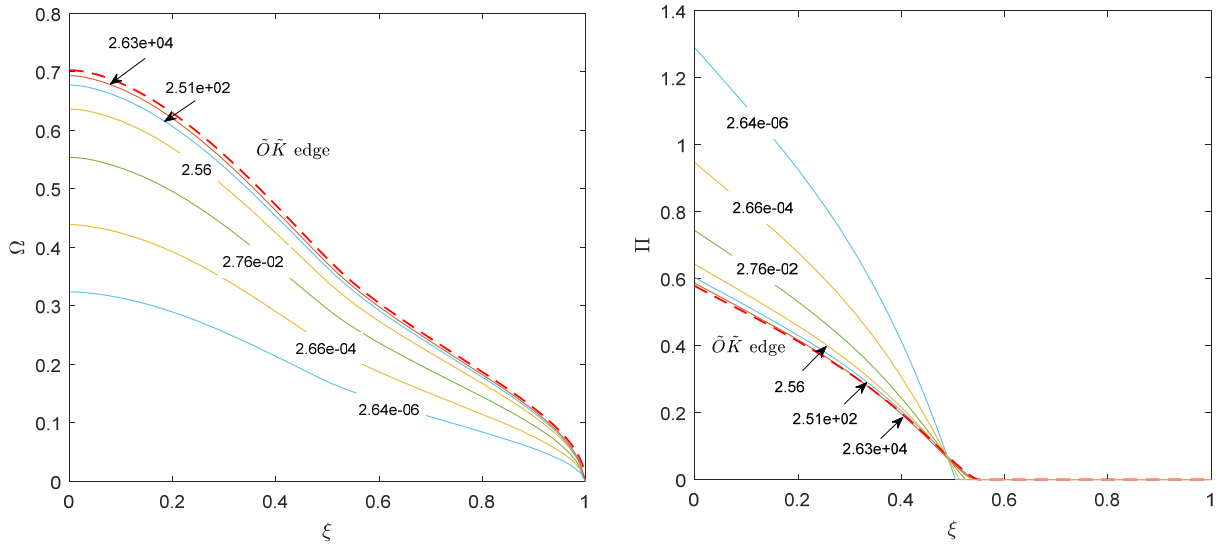


Figure 8. Evolution of the normalized fracture width (Left) and normalized fluid pressure (Right) under zero dimensionless confining stress and $\mathcal{K}=0.498$. Solid lines represent the numerical solutions at different dimensionless time $t/t_l$ and the dashed line represents the self-similar solution at $\tilde{O}\tilde{K}$ edge

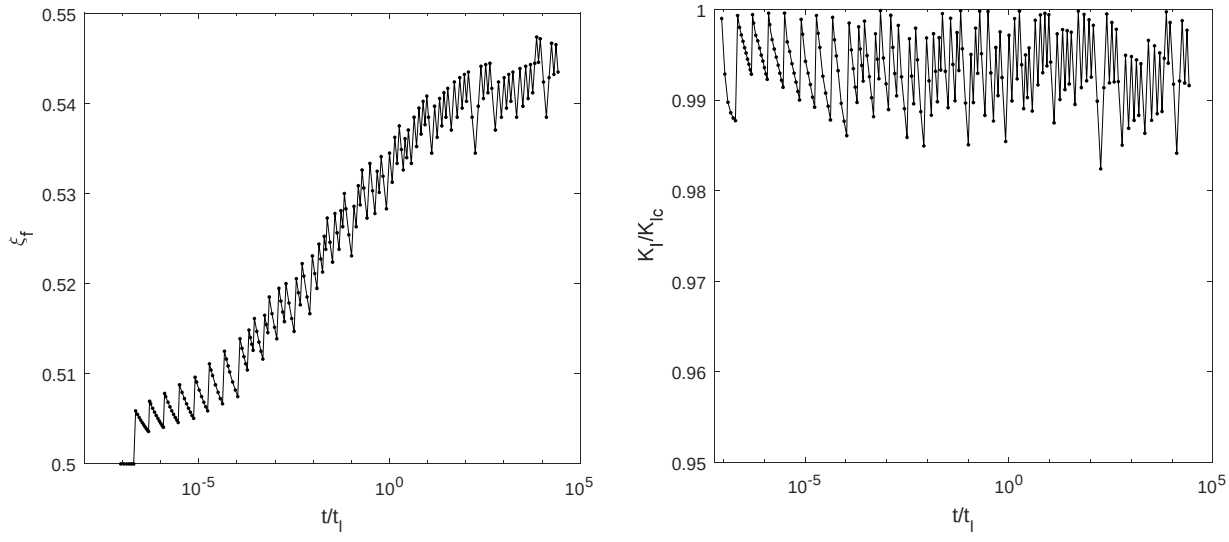


Figure 9. Evolution of ratio of fluid fraction (Left) and ratio of stress intensity factor to rock toughness (Right)

### 5.3 Different propagation regimes from OK edge to $\widetilde{M}\widetilde{K}$ edge

In the case where the relative magnitude of the time scale $\mathcal{R} = 1$ or $\mathcal{R} \gg 1$, the state of hydraulic fracturing would follow the path from plane $OK\widetilde{O}\widetilde{K}$ to plane $\widetilde{O}\widetilde{M}\widetilde{K}$ or from plane OMK to plane $MK\widetilde{M}\widetilde{K}$. In more general case where $\mathcal{R}$ is slightly over or below 1, it would follow a curved path on a plane parallel to plane $OM\widetilde{O}\widetilde{M}$ with specific dimensionless toughness. Depending on the relative magnitude of the two time scale, the path may be close to the line connecting OK edge and $\widetilde{M}\widetilde{K}$ edge or bend to $\widetilde{O}\widetilde{K}$ edge or MK edge. In the following part, hydraulic fracturing processes with the same dimensionless toughness $\mathcal{K} = 0.5$ and different $\mathcal{R}$ are simulated with the finite element model detailed in Section 4. The related parameters for the numerical cases are listed in Table 3.

Table 3 Rock properties, fluid properties and loading conditions used in numerical simulation

| Rock properties | | Fluid properties | | Loading conditions | | Leak-off coefficient |
|---|---|---|---|---|---|---|
| Elastic modulus | 45GPa | Viscosity | 10cp | | | Case 1: $1\times10^{-3}$ m/s$^{1/2}$ |
| Poisson ratio | 0.25 | Flow rate | 0.001m$^2$/s | $\sigma_0$ | 50MPa | Case 2: $5\times10^{-4}$ m/s$^{1/2}$ |
| Toughness | 1.68MPa • m$^{1/2}$ | | | | | Case 3: $2\times10^{-4}$ m/s$^{1/2}$ |

For the first case, the evolution of the fracture length is shown in Figure 10 and is compared with the limiting propagation regimes at OK edge and $\widetilde{M}\widetilde{K}$ edge. In the case $\mathcal{K} = 0.5$, half-length of the fracture at $\widetilde{M}\widetilde{K}$ edge evolves with time as:

$$l = L\gamma = \frac{1}{\pi}\left(\frac{Q_0^2 t}{C'^2}\right)^{1/2} \tag{40}$$

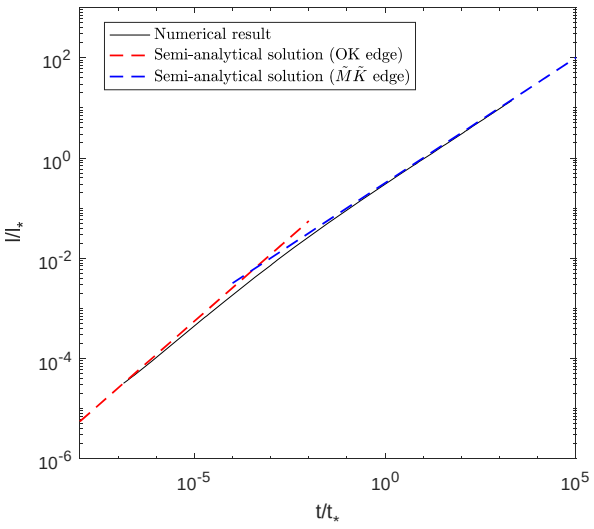


Figure 10. Evolution of the fracture half-length with respect to dimensionless time under non-zero dimensionless confining stress

Figure 11 plots the hydraulic fracture path in the parametric space. The parametric plane for $\mathcal{K} = 0.5$ can be defined by $(\xi_f, r_f)$, where $\xi_f$ ranges from 0.5 to 1 and $r_f$ ranging from 0 to 1 denotes the ratio of fluid

volume stored in fracture to the total volume of fluid injected. The four vertices of the domain correspond to the point at which $\mathcal{K} = 0.5$ on edge OK, MK, $\widetilde{\mathrm{M}}\widetilde{\mathrm{K}}$ and $\widetilde{\mathrm{O}}\widetilde{\mathrm{K}}$ respectively (from (0.5, 1) to (0.5,0) in clockwise direction). The value of $\mathcal{R}$ is computed as

$$\mathcal{R} = \frac{t_l}{t_\sigma} = \left( \frac{\sigma_0 Q_0}{E' C'^2} \right)^3 = 0.0177 \tag{41}$$

As expected, the hydraulic fracturing path evolves from the OK edge at early-time stage to the $\widetilde{\mathrm{M}}\widetilde{\mathrm{K}}$ edge in the end but bends to the $\widetilde{\mathrm{O}}\widetilde{\mathrm{K}}$ edge during the process since $t_l$ is smaller than $t_\sigma$. With the propagation of hydraulic fracture, the fluid fraction approximate to unit. On the aspect of fluid storage, the propagation regime changes from the storage-dominated regime on the top boundary to the leak-off-dominated regime on the bottom boundary.

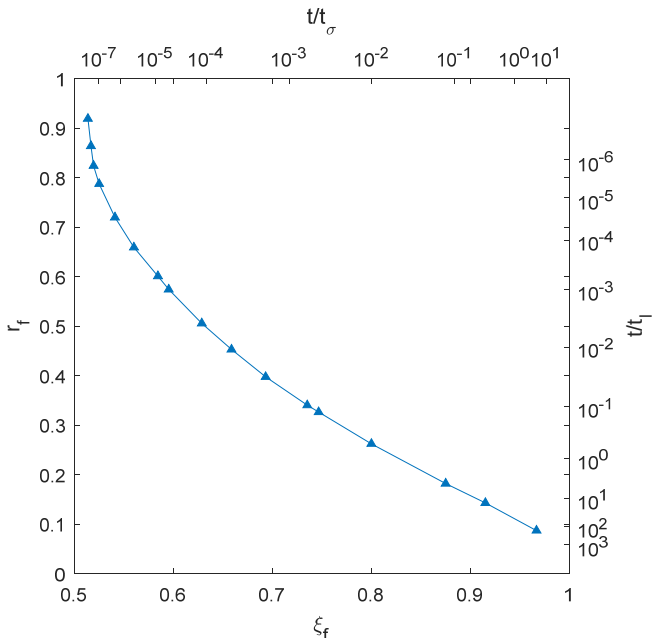


Figure 11. Hydraulic fracture path in the case of $\mathcal{K} = 0.5$ and $\mathcal{R} = 0.0177$

In order to check the relation between the dimensionless parameter $\mathcal{R}$ (i.e. the ratio of the two time scale) and the corresponding path in the parametric space, another two numerical cases with larger values of $\mathcal{R}$ are presented. The corresponding paths are compared in Figure 13. The dimensionless time are not shown due to the slight difference between the correspondence between $(\xi_f, r_f)$ and $(t/t_\sigma, t/t_l)$ for different value of $\mathcal{R}$.

As shown in Figure 12, the path for $\mathcal{R} = 1.13$ does not get close to the edge MK and $\widetilde{\mathrm{O}}\widetilde{\mathrm{K}}$ due to the small difference between the two time scales while the path bends to $\widetilde{\mathrm{O}}\widetilde{\mathrm{K}}$ edge (0.5, 0) for smaller $\mathcal{R}$ and MK edge (1, 1) for larger $\mathcal{R}$, which indicates that the dimensionless parameter $\mathcal{R}$ has a critical effect on the behavior of hydraulic fracturing.

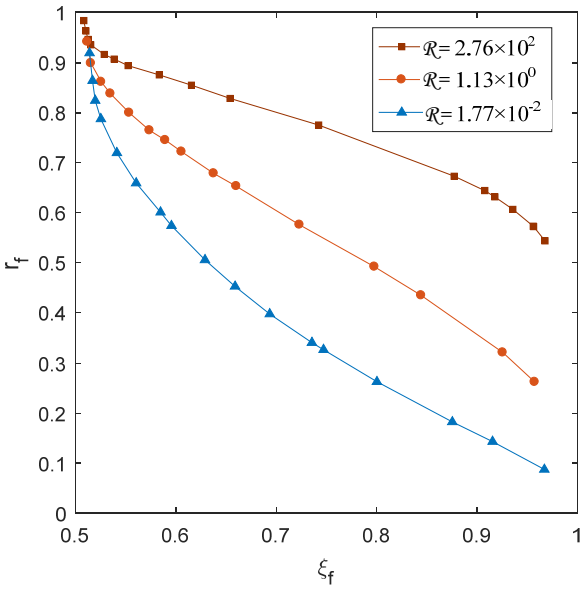


Figure 12. Hydraulic fracturing paths in the case of $\mathcal{K} = 0.5$ and various value of $\mathcal{R}$

## 6. Conclusions

In this paper, the propagation of a hydraulic fracture with a fluid lag in an infinite linear elastic permeable medium is investigated with both analytical and numerical approaches. Based on the KGD scheme, a new self-similar solution of leak-off dominated hydraulic fracturing is solved in a semi-analytical way firstly. Then a finite element based model is developed to verify the self-similar solution and to investigate the propagation regimes of hydraulic fracture in more general cases (with both fluid lag and leak-off). The main conclusions of this work are summarized below:

(1) On the analytical aspect, the general form of normalized governing equations with both fluid lag and leak-off considered is derived firstly. Then the self-similar solution in the limiting case of zero dimensionless confining stress ($\mathcal{T} = 0$) and infinite dimensionless leak-off coefficient ($\mathcal{L} = \infty$) ($\widetilde{\mathrm{OK}}$ edge in parametric space OMK-$\widetilde{\mathrm{OMK}}$) is solved in a semi-analytical way while existing analytical and numerical studies only focus on the case with fluid lag or leak-off separately (on OMK or MK$\widetilde{\mathrm{MK}}$ plane). The half-length, fluid net-pressure and fracture width are expressed as, $l(t) = \left(Q_0^2 t / C'^2\right)^{1/2} \gamma(\mathcal{K})$, $p(x,t) = \left(\mu' C'^2 E'^3 / Q_0 t\right)^{1/4} \Pi(\mathcal{K}, \xi)$ and $w(x,t) = \left(\mu' Q_0^3 t / E' C'^2\right)^{1/4} \Omega(\mathcal{K}, \xi)$, respectively. The self-similar solutions at $\widetilde{\mathrm{OK}}$ edge have a similar form as the solutions for OK edge but a higher dimensionless toughness $\mathcal{K}$ is observed in the case of the same fluid fraction $\xi_f$. The new self-similar solutions can be regarded as benchmarks for other hydraulic fracture models.

(2) A new dimensionless parameter $\mathcal{R}$, the ratio of the two time scale emerging in dimensionless confining stress $\mathcal{T}$ and dimensionless leak-off coefficient $\mathcal{L}$ is proposed to determine the hydraulic fracturing path in parametric space along with the dimensionless toughness $\mathcal{K}$. In the case $\mathcal{R} \gg 1$, hydraulic fracturing evolves from OK edge to MK edge firstly and then to $\widetilde{\mathrm{MK}}$ edge. Conversely, it evolves from OK edge to $\widetilde{\mathrm{OK}}$ edge and then to $\widetilde{\mathrm{MK}}$ edge in case of $\mathcal{R} = 1$. In more general cases $\mathcal{R}$ is slightly over 1 (or below 1), hydraulic fracturing paths would only bend to MK edge (or $\widetilde{\mathrm{OK}}$ edge) but keep always from them.

(3) On the numerical aspect, a robust finite element based KGD model is developed to simulate the propagation of hydraulic fracture with both the fluid lag and leak-off considered. Both the rock deformation and fluid flow are discretized with finite elements and are solved together using the Newton-Raphson method. It is found that the explicit time step leads to unstable fluid front velocity in the case of low fluid front velocity due to significant leak-off. The time step in our model is determined implicitly to avoid the fluctuation of fluid front velocity, which makes the program very robust. The transient process from OK edge to $\widetilde{\mathrm{O}}\widetilde{\mathrm{K}}$ edge is simulated and the approximation of the numerical solutions to the self-similar solutions at $\widetilde{\mathrm{O}}\widetilde{\mathrm{K}}$ edge are observed, which verifies the accuracy of the self-similar solution. A more general process from OK edge to $\widetilde{\mathrm{M}}\widetilde{\mathrm{K}}$ edge for various values of $\mathcal{R}$ are simulated. The effectiveness of the proposed dimensionless parameter $\mathcal{R}$ is proved. These findings help to understand the various propagation regimes of hydraulic fracture.

## Acknowledgement

The authors would like to thank the support from the European Community's Seventh Framework Programme (Marie Curie International Research Staff Exchange Scheme, Grant No. 612607), the Sêr Cymru National Research Network in Advanced Engineering and Materials, the China Scholarship Council, the Welsh Government Sêr Cymru Programme, the Robert A. Welch Foundation (C-0002) and the Royal Academy of Engineering.

## References

[1]Lecampion B, Detournay E. An implicit algorithm for the propagation of a hydraulic fracture with a fluid lag. Computer Methods in Applied Mechanics and Engineering 2007; **196**(49-52):4863-4880.

[2]Adachi JI, Detournay E. Plane strain propagation of a hydraulic fracture in a permeable rock. Engineering Fracture Mechanics 2008; **75**(16):4666-4694.

[3]Garagash DI. Plane-strain propagation of a fluid-driven fracture during injection and shut-in: Asymptotics of large toughness. Engineering Fracture Mechanics 2006; **73**(4):456-481.

[4]Khristianovic SA, Zheltov YP. Formation of Vertical Fractures by Means of Highly Viscous Liquid. 4th World Petroleum Congress, Rome, Italy, 1955.

[5]Geertsma J, De Klerk F. A Rapid Method of Predicting Width and Extent of Hydraulically Induced Fractures. Journal of Petroleum Technology 1969; **21**(12):1571-1581.

[6]Carbonell R, Desroches J, Detournay E. A comparison between a semi-analytical and a numerical solution of a two-dimensional hydraulic fracture. International Journal of Solids and Structures 1999; **36**(31–32):4869-4888.

[7]Spence DA, Sharp P. Self-Similar Solutions for Elastohydrodynamic Cavity Flow. Proceedings of the Royal Society A: Mathematical, Physical and Engineering Sciences 1985; **400**(1819):289-313.

[8]Adachi JI, Detournay E. Self-similar solution of a plane-strain fracture driven by a power-law fluid. International Journal for Numerical and Analytical Methods in Geomechanics 2002; **26**(6):579-604.

[9]Garagash DI, Detournay E. Plane-Strain Propagation of a Fluid-Driven Fracture: Small Toughness Solution. Journal of Applied Mechanics 2005; **72**(6):916-928.

[10]Garagash DI. Propagation of a plane-strain hydraulic fracture with a fluid lag: Early-time solution. International Journal of Solids and Structures 2006; **43**(18-19):5811-5835.

[11]Hu J, Garagash DI. Plane-Strain Propagation of a Fluid-Driven Crack in a Permeable Rock with Fracture Toughness. Journal of Engineering Mechanics 2010; **136**(9):1152-1166.

[12]Wang Z-Q, Detournay E. The Tip Region of a Near-Surface Hydraulic Fracture. Journal of Applied Mechanics 2018; **85**(4):041010.

[13]Detournay E. Mechanics of Hydraulic Fractures. Annual Review of Fluid Mechanics 2016; **48**(1):311-339.

[14]Adachi JI, Detournay E, Garagash DI, Savitski AA, Interpretation and design of hydraulic fracturing treatments. 2004, Google Patents.

[15]Bunger AP, Detournay E, Garagash DI. Toughness-dominated Hydraulic Fracture with Leak-off. International Journal of Fracture 2005; **134**(2):175-190.

[16]Dong XL, Zhang GQ, Gao DL, Duan ZY. Toughness-Dominated Hydraulic Fracture in Permeable Rocks. Journal of Applied Mechanics-Transactions of the Asme 2017; **84**(7):071001.

[17]Garagash D. Hydraulic Fracture Propagation in Elastic Rock With Large Toughness. 4th North American Rock Mechanics Symposium, Seattle, Washington, 2000.

[18]Haddad M, Sepehrnoori K. XFEM-Based CZM for the Simulation of 3D Multiple-Cluster Hydraulic Fracturing in Quasi-Brittle Shale Formations. Rock Mechanics and Rock Engineering 2016; **49**(12):4731-4748.

[19]Wang T, Liu Z, Zeng Q, Gao Y, Zhuang Z. XFEM modeling of hydraulic fracture in porous rocks with natural fractures. Science China Physics, Mechanics & Astronomy 2017; **60**(8).

[20]Santillán D, Juanes R, Cueto-Felgueroso L. Phase field model of fluid-driven fracture in elastic media: Immersed-fracture formulation and validation with analytical solutions. Journal of Geophysical Research: Solid Earth 2017; **122**(4):2565-2589.

[21]Wang T, Liu Z, Gao Y, Zeng Q, Zhuang Z. Theoretical and Numerical Models to Predict Fracking Debonding Zone and Optimize Perforation Cluster Spacing in Layered Shale. Journal of Applied Mechanics 2017; **85**(1):011001.

[22]Zeng Q, Liu Z, Wang T, Gao Y, Zhuang Z. Fully coupled simulation of multiple hydraulic fractures to propagate simultaneously from a perforated horizontal wellbore. Computational Mechanics 2017.

[23]Dontsov EV. An approximate solution for a plane strain hydraulic fracture that accounts for fracture toughness, fluid viscosity, and leak-off. International Journal of Fracture 2017; **205**(2):221-237.

[24]Detournay E, Hakobyan Y, Eve R. Self-Similar Propagation of a Hydraulic Fracture in a Poroelastic Medium. in Poromechanics 2017-Proceedings of the 6th Biot Conference on Poromechanics. 2017. American Society of Civil Engineers (ASCE).

[25]Huynen A, Detournay E. Self-Similar Propagation of a Plastic Zone Due to Fluid Injection in a Porous Medium. in Poromechanics 2017 - Proceedings of the 6th Biot Conference on Poromechanics 2017. American Society of Civil Engineers (ASCE).

[26]Desroches J, Thiercelin M. Modelling the propagation and closure of micro-hydraulic fractures.

International Journal of Rock Mechanics and Mining Sciences & Geomechanics Abstracts 1993; **30**(7):1231-1234.

[27]Detournay E. Propagation Regimes of Fluid-Driven Fractures in Impermeable Rocks. International Journal of Geomechanics 2004; **4**(1):35-45.

[28]Hunsweck MJ, Shen Y, Lew AJ. A finite element approach to the simulation of hydraulic fractures with lag. International Journal for Numerical and Analytical Methods in Geomechanics 2013; **37**(9):993-1015.

[29]Walters MC, Paulino GH, Dodds RH. Interaction integral procedures for 3-D curved cracks including surface tractions. Engineering Fracture Mechanics 2005; **72**(11):1635-1663.